nature physics

Article

https://doi.org/10.1038/s41567-025-02813-z

Detection of fractional quantum Hall states by entropy-sensitive measurements

Received: 21 June 2024

Accepted: 29 January 2025

Published online: 17 March 2025

Check for updates

Nishat Sultana[1], Robert W. Rienstra[1], Kenji Watanabe[2], Takashi Taniguchi[3], Joseph A. Stroscio[4], Nikolai B. Zhitenev[4], D. E. Feldman[5] & Fereshte Ghahari[1]

The thermopower of a clean two-dimensional electron system is directly proportional to the entropy per charge carrier and can probe strongly interacting quantum phases such as fractional quantum Hall liquids. In particular, thermopower is a valuable parameter to probe the quasiparticle statistics that give rise to excess entropy in certain even-denominator fractional quantum Hall states. Here we demonstrate that the magneto-thermopower detection of fractional quantum Hall states is more sensitive than resistivity measurements. We do this in the context of Bernal-stacked bilayer graphene and highlight several even-denominator states at a relatively low magnetic field. These capabilities of thermopower measurements support the interest in fractional quantum Hall states for finding quasiparticles with non-Abelian statistics and elevate bilayer graphene as a promising platform for achieving this.

The fractional quantum Hall effect (FQHE) is a hallmark of strong interactions in two-dimensional electron systems in the presence of large magnetic fields[1]. Of particular importance among the plethora of fractional quantum Hall (FQH) states are specific even-denominator states that are expected to exhibit non-Abelian statistics. One such state is the state observed at filling factor $\nu = 5/2$ in GaAs, which has been the subject of intensive research since its discovery[2] for its potential applications in fault-tolerant quantum computation[3,4]. The observed gap in this state can be explained by the Cooper pairing of composite fermions[5,6]. However, depending on the types of pairing, the ground state and topological order can be different. These different possibilities, including eight Abelian and eight non-Abelian pairing states, are known as the topological orders of the 16-fold way[7,8]. Although the leading numerical calculations propose the ground state to be the non-Abelian Moore–Read, Pfaffian (Pf) or anti-Pf state, the experiments seem to be consistent with the non-Abelian particle–hole-symmetric Pf state[7]. Despite intense experimental interest, it is hard to narrow down the topological order to a single state[8]. A small energy gap poses a major challenge for the understanding of the fragile half-integer states in GaAs. A brighter strategy is to, thus, focus on alternate materials with an even more robust FQHE, such as bilayer graphene (BLG).

FQHE in BLG

Beyond GaAs, FQH states at half-filling have been observed in other systems[9–21]. Specifically, BLG has recently emerged as a new platform to study even-denominator states. The zeroth Landau level (LL) in this system supports a rich variety of interaction-induced states. This diversity arises from an eight-fold degeneracy involving the $N = 0$ and $N = 1$ orbitals and the possible spin and valley isospin combinations thereof. In recent experiments[16,17], a series of robust and tunable even-denominator FQH states has been observed at the half-filling of symmetry-broken states with orbital index $N = 1$, whereas no strong evidence of such states has been detected in the $N = 0$ orbital branches. These states are consistent with theoretical expectations[22–24] to be either a Pf or anti-Pf state due to the qualitative similarity to the $\nu = 5/2$ state in GaAs, which also appears in the $N = 1$ LL. However, these previous studies were primarily focused on conventional transport and compressibility measurements[16,17]. Thermopower experiments to study FQH states in graphene and its bilayer are currently lacking.

[1]Department of Physics and Astronomy, George Mason University, Fairfax, VA, USA. [2]Research Center for Electronic and Optical Materials, National Institute for Materials Science, Tsukuba, Japan. [3]Research Center for Materials Nanoarchitectonics, National Institute for Materials Science, Tsukuba, Japan. [4]Physical Measurement Laboratory, National Institute of Standards and Technology, Gaithersburg, MD, USA. [5]Theoretical Physics Center and Physics Department, Brown University, Providence, RI, USA. e-mail: fghahari@gmu.edu

As we demonstrate below, these measurements are more powerful probes of FQH states in these systems.

Thermopower measurements

The conversion of heat into electricity is known as the thermoelectric effect. A particular form of thermoelectricity is thermopower, also known as the Seebeck effect. In a thermopower measurement, a temperature gradient ΔT is applied to a material, which causes a thermal diffusion current to migrate from the hotter end towards the colder end, which produces an excess of charge accumulating at the ends of the device. When no net current is flowing, the system establishes a uniform electric field antiparallel to ΔT, which results in a detectable thermoelectric voltage ΔV across the sample. The thermopower S is then simply defined as $S = -\Delta V/\Delta T$.

It is known that the thermopower, a transport coefficient, is related to the entropy per charge carrier—a thermodynamic variable. Specifically, it has been shown for non-interacting systems that the thermopower is given by[25]

$$S = s/qn, \tag{1}$$

where q is the carrier charge ($q = -e$ in the case of electrons), s is the entropy and n is the carrier density. This relation also holds for interacting electrons even in high magnetic fields[26,27]. This entropic connection makes thermopower a powerful alternative tool to probe the topological order since the entropy carried by non-Abelian quasiparticles is predicted to be anomalously larger than that of Abelian quasiparticles[26]. As of now, there are limited thermopower studies of the $\nu = 5/2$ state in GaAs (refs. 28,29). Furthermore, phonon-drag contribution leading to a non-monotonic temperature dependence of thermopower already appears in temperatures as low as 200 mK in GaAs, limiting the thermopower measurements to very low temperatures[28,29]. By contrast, phonon-drag thermopower is negligible in graphene-based systems due to the weak electron–phonon coupling, making them ideal platforms to study FQH states at broader temperature ranges[30–38].

In this Article, we report the thermopower measurements of FQH states in Bernal-stacked BLG, where we detect even-denominator FQH states at the $N = 0$ LL in the measured thermal signal. Our data indicate that thermopower as a measure of entropy is a more sensitive probe of FQH states compared with resistivity measurements.

In this work, we utilize metal resistance thermometry, which is suitable for the nanoscale devices measured here[32,39]. An optical image of a typical graphene thermoelectric device produced by the stacking of van der Waals materials is shown in Fig. 1a. A controlled temperature gradient ΔT is applied to the sample by a microfabricated heater, and the resulting thermally induced voltage ΔV is measured by the voltage probes to evaluate the thermopower (Fig. 1b). Local temperature variations are measured using two metal four-probe thermometers followed by temperature calibration (Supplementary Fig. 1).

Figure 1c,d displays the longitudinal component (Seebeck coefficient), S_{xx}, and the transverse component (Nernst signal), S_{xy}, of thermopower versus filling factor $\nu = \frac{nh}{eB}$ measured at 2 T for BLG device no. 1. For comparison, the corresponding measured resistivity components R_{xx} and R_{xy} are plotted on these graphs. The minima in S_{xx} are well aligned with those in R_{xx} associated with various QH states, as well as with the quantized plateaus in R_{xy}. The dashed lines positioned between the LLs where the thermopower goes to zero represent well-developed QH states at $\nu = \pm4, \pm8, \pm12\ldots$, characteristic of the integer quantum Hall (IQH) effect in BLG. Both components vanish between LLs at which no carriers are available to participate in diffusion, whereas they take finite values as the Fermi energy lies within the LLs. The Seebeck coefficient changes sign as the carrier density changes from electrons to holes and is the maximum at the centre of each LL. By contrast, the Nernst signal is symmetric relative to charge neutrality and has negative or positive values when the Fermi energy is below or above the centre of the LLs.

Figure 1e presents the Landau fan diagram of S_{xx} versus back-gate voltage and magnetic field. By increasing the magnetic field, symmetry-broken states within each LL become well resolved in fields as small as 3–6 T, leading to additional QH states at $\nu = \pm1, \pm2, \pm3, \pm5, \pm6, \pm7\ldots$, an indication of the high quality of our devices. Figure 1f displays the line cuts of S_{xx} versus ν at different magnetic fields, showing the evolution of the peak values with magnetic field. The thermopower decreases as the field increases due to interaction-induced ordering as the symmetry-broken states and FQH states are being resolved.

For a quantitative evaluation of the measured data, we apply the semiclassical formalism. For a non-interacting electron system in the presence of disorder, as long as $k_B T \ll \Gamma$ (where Γ is the LL broadening), the thermopower can be approximated by the generalized Mott formula given by

$$S_{ij}^{\mathrm{Mott}} = \frac{\pi^2 k_B^2 T}{3|e|} \sum_k (\sigma^{-1})_{ik} \left(\frac{\partial \sigma}{\partial E_f}\right)_{kj}, \tag{2}$$

where e is the electron charge and k_B is the Boltzmann constant[40–42]. Moreover, σ_{ij} is the conductivity tensor and E_f is the Fermi energy. Although this relation qualitatively predicts the basic features of diffusion thermopower in the IQH regime (Fig. 1c,d), our measured thermopower considerably overestimates these predictions (Supplementary Fig. 5). A closer examination of our data shows better agreement with general entropic models of thermopower measurements (Supplementary Section B)[25,40,43,44].

We now turn our attention to thermopower measurements in the FQH regime. At higher magnetic fields, various FQH states emerge in addition to the symmetry-broken states. Figure 2a shows S_{xx} versus ν for electrons measured at 1.6 K. In addition to the symmetry-broken states, additional minima at fractional fillings are observable. The traces at different magnetic fields collapse onto a single universal curve with a strong minimum developed at $\nu = 1/2$ and weaker features around $\nu = 3/2$ and $\nu = 5/2$ and a few other fractions. Near integer filling factors, S_{xx} can become negative and display additional oscillations. Such oscillations, which were observed in previous experiments, can have various origins[27,41,45–47]. In our thermopower data from device no. 3 (Extended Data Fig. 1), these fluctuations are much smaller. Although the strong FQH state at $\nu = 1/2$ is apparent, a further differentiator of the FQH states from random oscillations is the behaviour of S_{xy} that should be crossing zero for well-developed states (similar to IQH states) or have a linear slope for states that are not fully developed. In Fig. 2b,c, we have presented S_{xy} on the same graph as S_{xx} around $\nu = 1/2$ and $\nu = 5/2$, which shows the expected linear slope, further proving the existence of these states. As shown in Fig. 2d, stronger FQH states appear specifically at even-denominator fractional fillings with weaker dips at other fractional fillings at a lower temperature of 300 mK. The FQH states are more pronounced on the electron side, with weaker FQH states on the hole side (Supplementary Fig. 21). This is attributed to the electron–hole asymmetry often observed in graphene devices due to disorder scattering. To further confirm the existence of FQH states, the Landau fan diagram of S_{xx} as a function of $\nu = nh/eB$ and magnetic field is presented in Fig. 2e (Supplementary Fig. 11b). In this plot, the QH states appear as vertical lines at specific filling factors, which makes their identification easier. In addition to symmetry-broken states, we observe states at fractional fillings at which the very robust even-denominator FQH states at $\nu = 1/2$ and $\nu = 5/2$ are developed in fields as low as 8 T. The FQH state at $\nu = 3/2$ appears more strongly in field-dependent measurements (Supplementary Fig. 13). Note that we observe slight deviations of the filling factor of the states from the vertical lines, consistent with previous studies[17,48]. These shifts can be attributed

https://doi.org/10.1038/s41567-025-02813-z

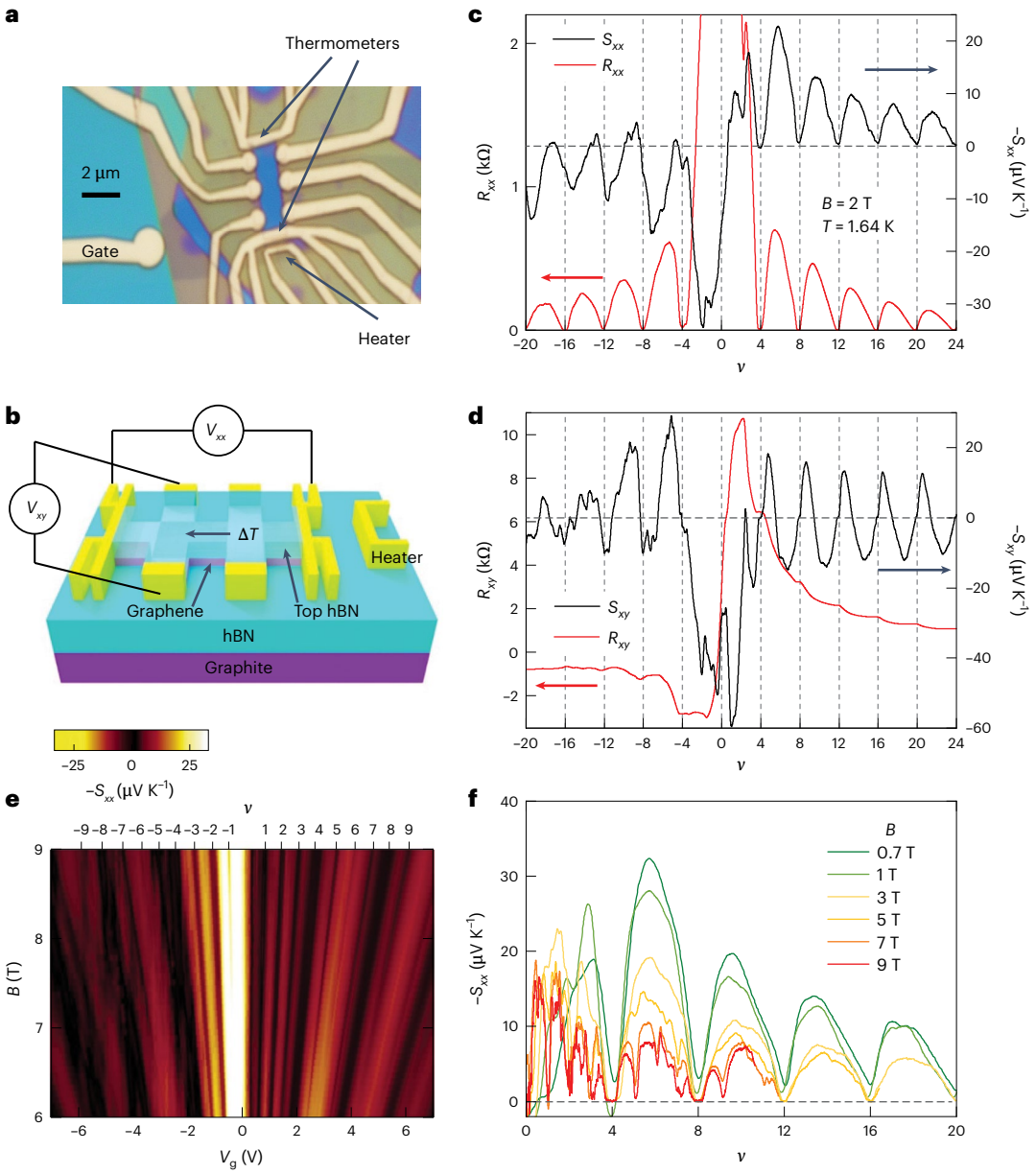

Fig. 1 | Thermopower measurements in the IQH regime. a, Optical image of an encapsulated BLG thermopower device with a graphite back gate. The arrows show the local thermometers and the heater. **b**, Schematic of the device and the thermopower measurement setup. The heater induces a temperature gradient across the sample. The longitudinal and transverse components of the thermal voltage are measured to obtain S_{xx} and S_{xy} in an applied magnetic field. hBN, hexagonal boron nitride. **c**, Longitudinal thermopower S_{xx} and longitudinal resistivity R_{xx}. **d**, Transverse thermopower S_{xy} and transverse resistivity R_{xy} as a function of ν at a fixed magnetic field $B = 2$ T and temperature $T = 1.64$ K. The vertical dotted lines represent filling factors corresponding to $\nu = \pm4, \pm8, \pm12\ldots$. **e**, Landau fan diagram of S_{xx} versus back-gate voltage and magnetic field. By increasing the magnetic field, symmetry-broken states within each LL are well resolved. The solid lines display quantum Hall states at $\nu = \pm1, \pm2, \pm3, \pm4, \pm5, \pm6, \pm7\ldots$. **f**, Line cuts of S_{xx} versus ν at different magnetic fields, showing that S_{xx} decreases with magnetic field as symmetry-broken states are being resolved.

either to the fluctuations of the charge neutrality point over time due to a prolonged temperature gradient present in the sample or to changes in quantum capacitance.

We also performed field-dependent thermopower measurements to further confirm the presence of FQH states. Figure 2f,g shows the plots of S_{xx} at a fixed density as the magnetic field changes at two temperatures of 300 mK and 1.64 K. In such measurements, the thermopower exhibits deep minima at various FQH states, including the well-developed states at $\nu = 1/2$ and $\nu = 5/2$.

Thermopower measurements in device no. 2 (Supplementary Fig. 11c) and device no. 3 (Extended Data Fig. 1) also provide convincing evidence for the existence of even-denominator states. The state at $\nu = 1/2$ is observed in device nos. 1 and 3, whereas the $\nu = 5/2$ state is observed in all three devices (Supplementary Fig. 12).

In particular, FQH states are far more pronounced in thermopower measurements (Fig. 2d) compared with resistivity measurements. In device no. 1 (Supplementary Fig. 7), the FQH states only appear as incipient states in resistivity. Stronger FQH states at $\nu = 7/5$ and $\nu = 5/2$ are observable in R_{xx} measurements in device no. 3 (Extended Data Fig. 1 and Supplementary Fig. 8); however, thermopower always displays more FQH states. For example, FQH states appear in thermopower at lower densities, whereas resistivity diverges near the charge neutrality point, making such measurements less sensitive to the FQH states in this regime. Overall, resistivity measurements vary in sensitivity to

https://doi.org/10.1038/s41567-025-02813-z

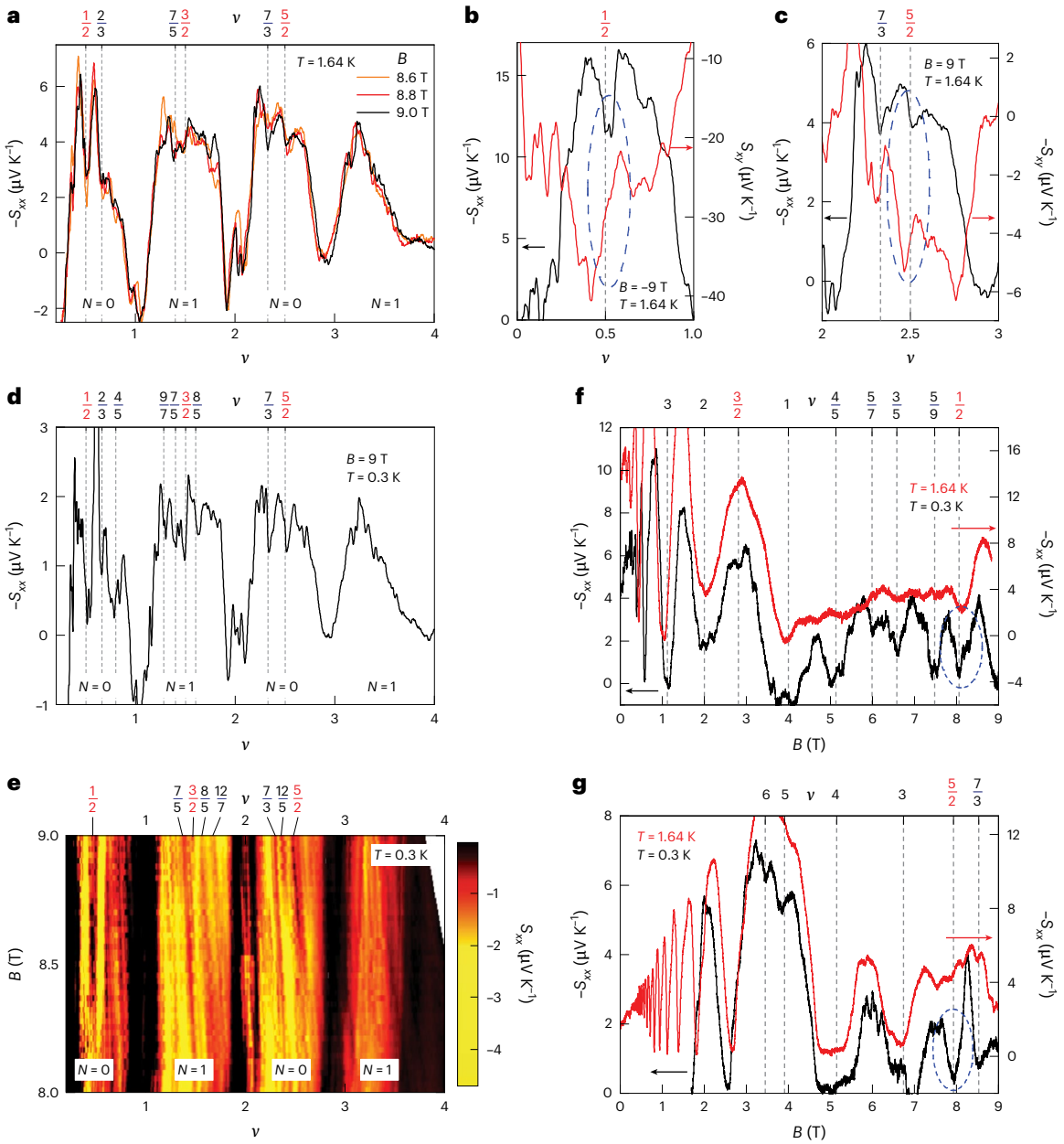

Fig. 2 | Thermopower measurements in the FQH regime. a, S_{xx} versus ν displaying a multitude of FQH states measured at magnetic fields of 8.6 T, 8.8 T and 9 T and $T = 1.64$ K for device no. 1. In BLG, LLs with orbital index $N = 0$ and $N = 1$ are degenerate in energy spanning $\nu = -4$ to 4. **b**, S_{xx} (black) and S_{xy} (red) measured at $T = 1.64$ K and $B = -9$ T around $\nu = 1/2$. **c**, S_{xx} (black) and S_{xy} (red) measured at $T = 1.64$ K and $B = 9$ T around $\nu = 5/2$ for device no. 1. S_{xx} shows minima at FQH states including $\nu = 1/2$ and $\nu = 5/2$, while S_{xy} shows a linear slope around these states (see the blue oval regions in **b** and **c**). **d**, S_{xx} versus ν measured at $B = 9$ T and $T = 300$ mK for device no. 1, showing FQH states appearing at even-denominator states and other fractional fillings. **e**, S_{xx} as a function of ν and magnetic field B measured at $T = 300$ mK for device no. 1. Slight shifts observed in the locations of the observed IQH and FQH states versus field are attributed to fluctuations in the charge neutrality point over time due to a prolonged temperature gradient present in the sample, potentially moving impurities around at our base temperature of 300 mK. **f**,**g**, S_{xx} versus magnetic field measured at a fixed density of $n = 0.99 \times 10^{11}$ cm^{-2} (**f**) and $n = 4.83 \times 10^{11}$ cm^{-2}(**g**) and temperatures of 300 mK and 1.64 K. FQH states including even-denominator states are more developed at lower temperatures and higher fields. The density is chosen such that the even-denominator states appear at the highest attainable field.

the FQH states between devices and contact pairs, but thermopower shows the same strong FQH states at $\nu = 1/2$ and $\nu = 5/2$ being the more sensitive and effective measurement method.

Generally, R_{xx} at filling factors corresponding to incompressible regions depends on the number of charged quasiparticles. In a realistic system, these quasiparticles emerge either by thermal activation or disorder. In the case that disorder is much larger than the energy gap, R_{xx} displays no signatures. A voltage gradient in the Seebeck effect also requires the presence of mobile charge carriers. Hence, S_{xx} and R_{xx} are both suppressed on quantum Hall plateaus. However, the Seebeck coefficient is also sensitive to the entropy density. Its suppression at low temperatures may result in deeper minima of S_{xx} compared with R_{xx}.

The relation between thermopower and resistivity is further explored by comparing the measured thermopower with the derivative of resistivity and the generalized Mott formula (Supplementary Fig. 9a,b). Although the basic features of diffusion thermopower in the IQH regime might qualitatively match, the traces look very dissimilar in the FQH regime. This further introduces thermopower as

https://doi.org/10.1038/s41567-025-02813-z

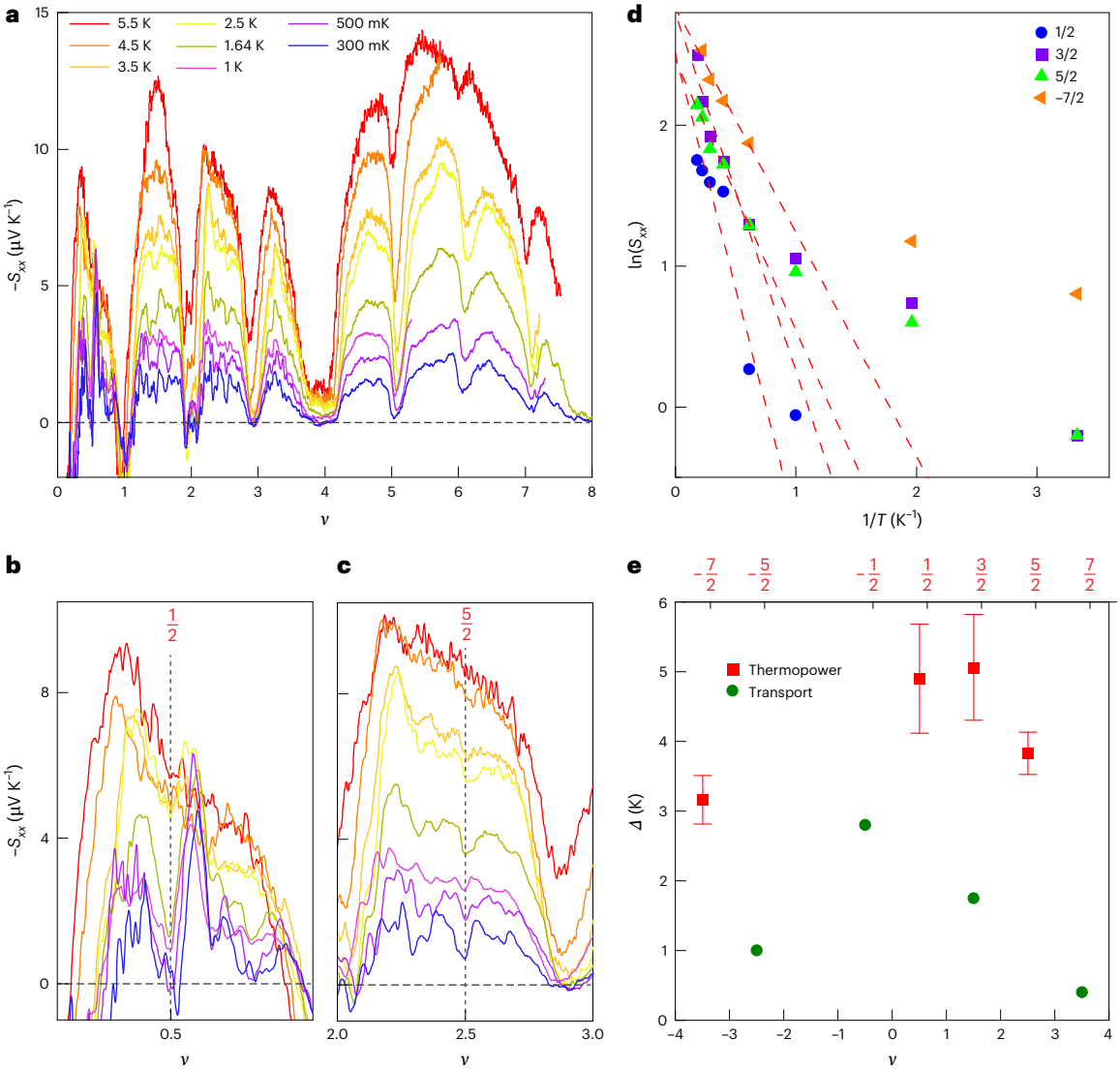

Fig. 3 | Energy gaps of even-denominator FQH states. a, S_{xx} versus ν measured at 9 T and various temperatures ranging from 300 mK to 5.5 K. S_{xx} decreases by reducing the temperature in both compressible and incompressible regions. **b**,**c**, Temperature-dependent S_{xx} around $\nu = 1/2$ (**b**) and $\nu = 5/2$ (**c**) measured at $B = 9$ T. **d**, Temperature dependence of S_{xx} at several even-denominator FQH states in an Arrhenius plot showing a simple activation behaviour at temperatures higher than 1 K. The energy gaps are extracted from the slope of the dashed lines. The error is smaller than the dot size for each data point in this graph. **e**, Energy gaps for various even-denominator states at 9 T extracted from thermopower measurements (square symbols) and compared with previous transport studies (circle symbols) where available[17]. The uncertainty represents one standard deviation from the linear least squares fits in **d**.

an independent probe of correlated states, which measures entropy rather than simply the derivative of resistivity.

One important feature of our thermopower data is that even-denominator states at the zeroth LL are strongly observed at the half-filling of symmetry-broken states with filling between $2k < \nu < 2k + 1$ ($k = 0$ and 1), in contrast to the previous experiments in BLG in which even-denominator states were only detected at the half-filling of symmetry-broken states with $2k + 1 < \nu < 2k + 2$ (refs. 16,17). In Fig. 2a,d,e, the orbital orderings are labelled based on the recent capacitance spectroscopic measurements of BLG[49] and our estimation of the displacement electric field (Supplementary Fig. 14). The symmetry-broken states with filling $2k < \nu < 2k + 1$ correspond to orbital index $N = 0$, whereas those with $2k + 1 < \nu < 2k + 2$ emerge from states with orbital index $N = 1$ (ref. 49). The appearance of an FQH state at $\nu = 5/2$ in $N = 0$ LL might be associated with the switching of orbital ordering to $N = 1$ LL at small displacement electric fields (<35 mV nm^{-1}), as suggested for the $\nu = 5/2$ state observed in a recent transport experiment[48]. However, the estimated magnitude of the displacement electric field in our devices is larger (~50 mV nm^{-1}) compared with this previous study[48], and another mechanism might be responsible for the appearance of this state in $N = 0$ LL. The latter explanation is also not applicable for the state we observe at $\nu = 1/2$. The states emerging at the half-filled $N = 0$ LL can alternatively be formed by a different mechanism. On the basis of theory, these states are consistent with $SU(2)_2$ or the so-called 221 parton state, which also supports a non-Abelian topological order[7,8,50]. This state is favoured to exist only at lower magnetic fields at which the LL mixing parameter is larger[50]. This is the case in our devices where the FQH states develop at relatively low magnetic fields compared with previous experiments. However, future experiments such as quasiparticle tunnelling and local thermometry measurements are required to directly distinguish this state from other candidates such as a particle–hole-symmetric Pf state.

To extend the characterization of FQH states at half-filling, we used temperature dependence measurements to estimate their energy gaps. Figure 3a displays the thermopower S_{xx} measured at 9 T for a sequence of different temperatures. As expected, the magnitude of S_{xx}

https://doi.org/10.1038/s41567-025-02813-z

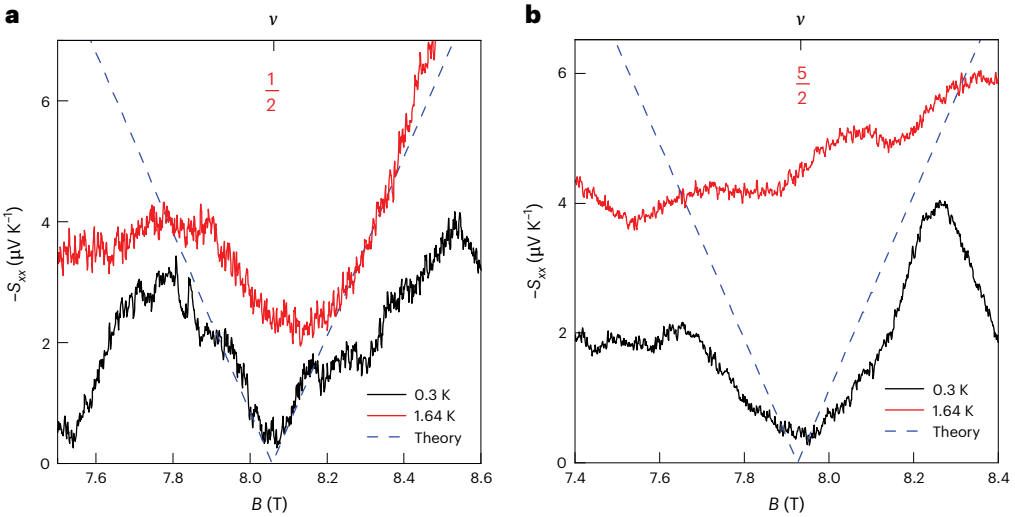

Fig. 4 | Excess entropy of even-denominator FQH states. a,**b**, Comparison between the thermopower predicted by YH theory[26] (dashed lines) following equation (3) and measured S_{xx} at around $\nu = 1/2$ (**a**) $\nu = 5/2$ (**b**) extracted from the measured data in Fig. 2f,g for temperatures of 300 mK and 1.64 K. The minima at these states fluctuates in the field from 1.64 K to 300 mK as charge neutrality moves slightly on cooling. The theoretical predictions are evaluated around the field at which these states appear at the base temperature of 300 mK.

decreases in compressible regions as the temperature reduces. This is in contrast with R_{xx} measurements in which the maxima of R_{xx} increase in magnitude as the temperature reduces.

Figure 3b,c shows the temperature dependence around $\nu = 1/2$ and $\nu = 5/2$ states, where the minima rapidly decrease with reducing temperature, consistent with a gapped state at these filling factors. The temperature dependence of the minimum of S_{xx} at several even-denominator FQH states is depicted in an Arrhenius plot (Fig. 3d), which shows a near activation (scaling as $\sim e^{-\Delta/2T}$) at temperatures higher than 1 K. At lower temperatures, a slower temperature dependence consistent with the variable-range hopping behaviour is observed. It is pointed out that this analysis is a very qualitative evaluation of the temperature dependence as the Arrhenius fit only works in a very narrow region, narrower than the one in our plots[51]. By comparing the size of the estimated energy gap for various even-denominator states, we observe that these gaps are larger than the gaps determined by previous transport measurements at higher fields for some fractions[17] (compare square and circle symbols in Fig. 3e), and are closer to recent activation-gap measurements of these states[52] but smaller than the thermodynamic gaps extracted from compressibility measurements at higher fields[16].

Finally, the relation between thermopower and entropy allows an investigation of the topological order of FQH states as the topological entropy originating from non-Abelian quasiparticle statistics is expected to dominate thermopower under certain conditions predicted by Yang and Halperin (YH)[26]. On the basis of this theory, the topological entropy gives rise to a temperature-independent thermopower given by

$$S = -\left|\frac{B-B_0}{B_0}\right|\left(\frac{k_B}{|e^*|}\right)\log[d], \qquad (3)$$

where B_0 is the magnetic field at which the FQH state appears, $d > 1$ is the quantum dimension and e^* is the quasiparticle charge. These predictions are expected to hold in a specific temperature range in which other sources of entropy excess can be ignored[26]. Although it is hard to quantify this temperature regime, it is estimated by YH theory to be between 7 mK and 300 mK for GaAs (ref. 26). A smaller dielectric constant in hexagonal-boron-nitride-encapsulated devices is expected to move the relevant window of energies up, making it plausible that the main source of entropy is topological for half-fillings at 300 mK.

To assess the predictions of equation (3), we evaluate the thermopower by using a quasiparticle charge of $e^* = 1/4$ and a quantum dimension of $d = \sqrt{2}$, as expected for a non-Abelian state of the 16-fold way[7]. Figure 4a,b displays a comparison between the predictions of YH theory[26] with experimental data around $\nu = 1/2$ and $\nu = 5/2$ at 300 mK and 1.64 K. Although the measured thermopower around $\nu = 5/2$ overestimates or underestimates the theoretical expectations (Fig. 4b), they are clearly in better quantitative agreement at $\nu = 1/2$ at 300 mK (Fig. 4a). This is suggestive of an excess topological entropy at $\nu = 1/2$, although further measurements are necessary to confirm this with greater certainty. To completely rule out the contributions from other sources of entropy access, thermopower measurements need to be performed over a broader temperature range in which a temperature-independent thermopower is anticipated. Furthermore, thermopower measurements in the Corbino geometry could be a more direct measure of quasiparticle entropy, as suggested elsewhere[53]. Overall, we expect future measurements performed in a wider temperature range and in a broader variety of devices can offer more information on the topological order of the observed FQH states.

Online content

Any methods, additional references, Nature Portfolio reporting summaries, source data, extended data, supplementary information, acknowledgements, peer review information; details of author contributions and competing interests; and statements of data and code availability are available at https://doi.org/10.1038/s41567-025-02813-z.

References

1. Tsui, D. C., Stormer, H. L. & Gossard, A. C. Two-dimensional magnetotransport in the extreme quantum limit. *Phys. Rev. Lett.* **48**, 1559–1562 (1982).
2. Willett, R. et al. Observation of an even-denominator quantum number in the fractional quantum Hall effect. *Phys. Rev. Lett.* **59**, 1776–1779 (1987).
3. Kitaev, A. Y. Fault-tolerant quantum computation by anyons. *Ann. Phys.* **303**, 2–30 (2003).
4. Nayak, C., Simon, S. H., Stern, A., Freedman, M. & Das Sarma, S. Non-Abelian anyons and topological quantum computation. *Rev. Mod. Phys.* **80**, 1083 (2008).

5. Jain, J. K. Composite-fermion approach for the fractional quantum Hall effect. *Phys. Rev. Lett.* **63**, 199–202 (1989).
6. Jain, J. K. *Composite Fermions* (Cambridge Univ. Press, 2007).
7. Feldman, D. E. & Halperin, B. I. Fractional charge and fractional statistics in the quantum Hall effects. *Rep. Prog. Phys.* **84**, 076501 (2021).
8. Ma, K. K. W. & Feldman, D. E. The sixteenfold way and the quantum Hall effect at half-integer filling factors. *Phys. Rev. B* **100**, 035302 (2019).
9. Suen, Y. W., Engel, L. W., Santos, M. B., Shayegan, M. & Tsui, D. C. Observation of a ν=1/2 fractional quantum Hall state in a double-layer electron system. *Phys. Rev. Lett.* **68**, 1379–1382 (1992).
10. Bolotin, K. I., Ghahari, F., Shulman, M. D., Stormer, H. L. & Kim, P. Observation of the fractional quantum Hall effect in graphene. *Nature* **462**, 196–199 (2009).
11. Du, X., Skachko, I., Duerr, F., Luican, A. & Andrei, E. Y. Fractional quantum Hall effect and insulating phase of Dirac electrons in graphene. *Nature* **462**, 192–195 (2009).
12. Ghahari, F., Zhao, Y., Cadden-Zimansky, P., Bolotin, K. & Kim, P. Measurement of the ν=1/3 fractional quantum Hall energy gap in suspended graphene. *Phys. Rev. Lett.* **106**, 046801 (2011).
13. Ki, D.-K., Fal'ko, V. I., Abanin, D. A. & Morpurgo, A. F. Observation of even denominator fractional quantum Hall effect in suspended bilayer graphene. *Nano Lett.* **14**, 2135–2139 (2014).
14. Kim, Y. et al. Fractional quantum Hall states in bilayer graphene probed by transconductance fluctuations. *Nano Lett.* **15**, 7445–7451 (2015).
15. Falson, J. et al. Even-denominator fractional quantum Hall physics in ZnO. *Nat. Phys.* **11**, 347–351 (2015).
16. Zibrov, A. A. et al. Tunable interacting composite fermion phases in a half-filled bilayer-graphene Landau level. *Nature* **549**, 360–364 (2017).
17. Li, J. I. A. et al. Even-denominator fractional quantum Hall states in bilayer graphene. *Science* **358**, 648–652 (2017).
18. Zibrov, A. A. et al. Even-denominator fractional quantum Hall states at an isospin transition in monolayer graphene. *Nat. Phys.* **14**, 930–935 (2018).
19. Falson, J. et al. A cascade of phase transitions in an orbitally mixed half-filled Landau level. *Sci. Adv.* **4**, eaat8742 (2018).
20. Kim, Y. et al. Even denominator fractional quantum Hall states in higher Landau levels of graphene. *Nat. Phys.* **15**, 154–158 (2019).
21. Shi, Q. et al. Odd- and even-denominator fractional quantum Hall states in monolayer WSe_2. *Nat. Nanotechnol.* **15**, 569–573 (2020).
22. Papić, Z., Abanin, D. A., Barlas, Y. & Bhatt, R. N. Tunable interactions and phase transitions in Dirac materials in a magnetic field. *Phys. Rev. B* **84**, 241306 (2011).
23. Apalkov, V. M. & Chakraborty, T. Stable Pfaffian state in bilayer graphene. *Phys. Rev. Lett.* **107**, 186803 (2011).
24. Papić, Z. & Abanin, D. A. Topological phases in the zeroth Landau level of bilayer graphene. *Phys. Rev. Lett.* **112**, 046602 (2014).
25. Obraztsov, Yu. N. The thermal EMF of semiconductors in a quantizing magnetic field. *Fiz. Tverd. Tela* **7**, 573–581 (1965).
26. Yang, K. & Halperin, B. I. Thermopower as a possible probe of non-Abelian quasiparticle statistics in fractional quantum Hall liquids. *Phys. Rev. B* **79**, 115317 (2009).
27. Cooper, N. R., Halperin, B. I. & Ruzin, I. M. Thermoelectric response of an interacting two-dimensional electron gas in a quantizing magnetic field. *Phys. Rev. B* **55**, 2344–2359 (1997).
28. Chickering, W. E., Eisenstein, J. P., Pfeiffer, L. N. & West, K. W. Thermoelectric response of fractional quantized Hall and reentrant insulating states in the N=1 Landau level. *Phys. Rev. B* **87**, 075302 (2013).
29. Chickering, W. E., Eisenstein, J. P., Pfeiffer, L. N. & West, K. W. Thermopower of two-dimensional electrons at filling factors ν=3/2 and 5/2. *Phys. Rev. B* **81**, 245319 (2010).
30. Bolotin, K. I., Sikes, K. J., Hone, J., Stormer, H. L. & Kim, P. Temperature-dependent transport in suspended graphene. *Phys. Rev. Lett.* **101**, 096802 (2008).
31. Hwang, E. H. & Das Sarma, S. Acoustic phonon scattering limited carrier mobility in two-dimensional extrinsic graphene. *Phys. Rev. B* **77**, 115449 (2008).
32. Zuev, Y. M., Chang, W. & Kim, P. Thermoelectric and magnetothermoelectric transport measurements of graphene. *Phys. Rev. Lett.* **102**, 096807 (2009).
33. Wei, P., Bao, W., Pu, Y., Lau, C. N. & Shi, J. Anomalous thermoelectric transport of Dirac particles in graphene. *Phys. Rev. Lett.* **102**, 166808 (2009).
34. Kim, D., Syers, P., Butch, N. P., Paglione, J. & Fuhrer, M. S. Ambipolar surface state thermoelectric power of topological insulator Bi_2Se_3. *Nano Lett.* **14**, 1701–1706 (2014).
35. Checkelsky, J. G. & Ong, N. P. Thermopower and Nernst effect in graphene in a magnetic field. *Phys. Rev. B* **80**, 081413 (2009).
36. Hwang, E. H., Rossi, E. & Das Sarma, S. Theory of thermopower in two-dimensional graphene. *Phys. Rev. B* **80**, 235415 (2009).
37. Nam, S.-G., Ki, D.-K. & Lee, H.-J. Thermoelectric transport of massive Dirac fermions in bilayer graphene. *Phys. Rev. B* **82**, 245416 (2010).
38. Ghahari, F. et al. Enhanced thermoelectric power in graphene: violation of the Mott relation by inelastic scattering. *Phys. Rev. Lett.* **116**, 136802 (2016).
39. Small, J. P., Perez, K. M. & Kim, P. Modulation of thermoelectric power of individual carbon nanotubes. *Phys. Rev. Lett.* **91**, 256801 (2003).
40. Girvin, S. M. & Jonson, M. Inversion layer thermopower in high magnetic field. *J. Phys. C: Solid State Phys.* **15**, L1147 (1982).
41. Gallagher, B. L. et al. Observation of universal thermopower fluctuations. *Phys. Rev. Lett.* **64**, 2058–2061 (1990).
42. Sultana, N. et al. Replication data for: detection of fractional quantum Hall states by entropic sensitive measurements. *George Mason University Dataverse* https://doi.org/10.13021/orc2020/681UPS (2024).
43. Oji, H. Thermopower and thermal conductivity in two-dimensional systems in a quantizing magnetic field. *Phys. Rev. B* **29**, 3148–3152 (1984).
44. Jonson, M. & Girvin, S. M. Thermoelectric effect in a weakly disordered inversion layer subject to a quantizing magnetic field. *Phys. Rev. B* **29**, 1939–1946 (1984).
45. Chickering, W. E. *Thermopower in Two-Dimensional Electron Systems*. PhD thesis, California Institute of Technology (2016).
46. Esposito, F. P., Goodman, B. & Ma, M. Thermoelectric power fluctuations. *Phys. Rev. B* **36**, 4507–4509 (1987).
47. Ilani, S. et al. The microscopic nature of localization in the quantum Hall effect. *Nature* **427**, 328 (2004).
48. Huang, K. et al. Valley isospin controlled fractional quantum Hall states in bilayer graphene. *Phys. Rev. X* **12**, 031019 (2022).
49. Hunt, B. M. et al. Direct measurement of discrete valley and orbital quantum numbers in bilayer graphene. *Nat. Commun.* **8**, 948 (2017).
50. Wu, Y.-H., Shi, T. & Jain, J. K. Non-Abelian parton fractional quantum Hall effect in multilayer graphene. *Nano Lett.* **17**, 4643–4647 (2017).
51. d'Ambrumenil, N., Halperin, B. I. & Morf, R. H. Model for dissipative conductance in fractional quantum Hall states. *Phys. Rev. Lett.* **106**, 126804 (2011).
52. Assouline, A. et al. Energy gap of the even-denominator fractional quantum Hall state in bilayer graphene. *Phys. Rev. Lett.* **132**, 046603 (2024).
53. Barlas, Y. & Yang, K. Thermopower of quantum Hall states in Corbino geometry as a measure of quasiparticle entropy. *Phys. Rev. B* **85**, 195107 (2012).

Data availability

The data that support the findings of this study are available from the George Mason University Dataverse at https://doi.org/10.13021/orc2020/681UPS (ref. 42). Source data are provided with this paper.

Acknowledgements

We thank Y. Barlas and F. Mahfouzi for useful discussions. N.S. acknowledges funding from the National Science foundation (NSF) under award no. 2337497. F.G. thanks J. Schnur for inspiring discussions and support. F.G. acknowledges funding from the National Institute of Standards and Technology (NIST) under grant no. 70NANB23H012. T.T. and K.W. acknowledge support from the Japan Society for the Promotion of Science KAKENHI under grant nos. 21H05233 and 23H02052 and World Premier International Research Center Initiative (WPI), Ministry of Education, Culture, Sports, Science and Technology (MEXT), Japan. D.E.F. was supported in part by the NSF under grant no. DMR-2204635.

Author contributions

F.G. conceptualized and designed the experiment. N.S. fabricated the devices. N.S. performed measurements and analysed the experimental data, under the supervision of F.G. R.W.R. assisted with data acquisition and cryostat maintenance. D.E.F. provided theoretical support of the experimental data. T.T. and K.W. grew the hexagonal boron nitride crystals. F.G., J.A.S. and N.B.Z. wrote the paper with input from all co-authors.

Competing interests

The authors declare no competing interests.

Additional information

Extended data is available for this paper at https://doi.org/10.1038/s41567-025-02813-z.

Supplementary information The online version contains supplementary material available at https://doi.org/10.1038/s41567-025-02813-z.

Correspondence and requests for materials should be addressed to Fereshte Ghahari.

Peer review information *Nature Physics* thanks the anonymous reviewers for their contribution to the peer review of this work.

https://doi.org/10.1038/s41567-025-02813-z

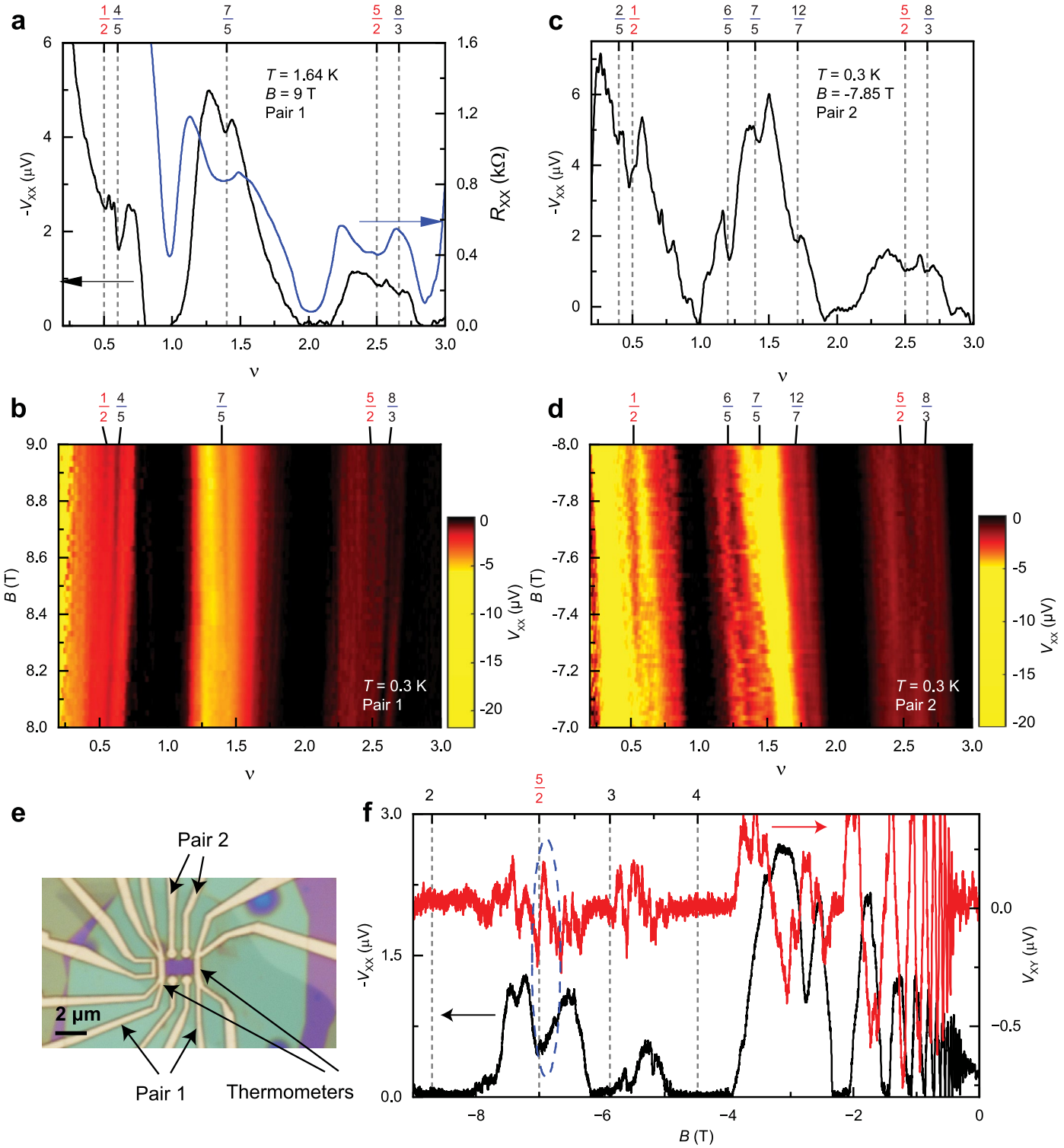

Extended Data Fig. 1 | Thermopower measurements in the fractional quantum Hall regime in device no. 3. a, The longitudinal thermal voltage V_{xx} (left axis) and R_{xx} (right axis) vs filling factor ν measured at $B = 9$ T and $T = 1.64$ K between pair 1 in device no. 3 (see **e**). While FQH states appear around filling factors 5/2 and 7/5 in R_{xx}, more FQH states are observable in V_{xx}. The temperature gradient was not calculated in this device due to a broken thermometer contact at base temperature. Therefore, the thermal voltage V_{xx} is plotted instead of thermopower. **b**, Landau fan of V_{xx} as a function of filling factor ν and magnetic field B at $T = 300$ mK measured between pair 1 in device no. 3 see **e**). In this plot the QH states appear as vertical lines at specific filling factors. In addition to integer QH states, FQH states at fractional fillings of 1/2, 4/5, 7/5, 5/2 and 8/3 are observable consistent with minima observed in **a**. **c**, Thermal voltage V_{xx} vs ν measured at $B = -7.85$ T and $T = 300$ mK between pair 2 in device no. 3 (see **e**). **d**, Landau fan of V_{xx} as a function of filling factor ν and magnetic field B measured at $T = 300$ mK between pair 2 showing vertical lines at fractional fillings including strong even denominator FQH states at 1/2 and 5/2 and odd denominator states consistent with those labeled in **c**. **e**, Optical image of a bilayer graphene thermopower device no. 3. Arrows show local thermometers and various electrode pairs used in measurements. **f**, V_{xx} and V_{xy} vs magnetic field B measured at fixed density of $n = 0.99 \times 1011\ \mathrm{cm}^{-2}$ at $T = 300$ mK between pair 1 showing a strong FQH state at ν = 5/2 specified by a minimum in V_{xx} (left axis) and a linear slope in V_{xy} (right axis) at this filling factor (see blue oval region). Only the strongest features are labeled.